

# Efficient Degradation of Methylene Blue by the Nano TiO<sub>2</sub>-functionalized Graphene Oxide Nanocomposite Photocatalyst for Wastewater Treatment

Ruibin Wang · Rendang Yang · Bin Wang ·  
Wenhua Gao

Received: 23 September 2015 / Accepted: 27 November 2015 / Published online: 2 December 2015  
© Springer International Publishing Switzerland 2015

**Abstract** Herein, an efficient nano TiO<sub>2</sub>-functionalized graphene oxide nanocomposite photocatalyst was readily prepared, using an ordinary solvothermal technique. It was noted that the as-prepared nanocomposite yielded a quadruple degradation capacity of the previously reported P25-graphene composite photocatalyst towards methylene blue (MB). To elucidate this, the Brunauer–Emmett–Teller (BET)-specific surface area, conductivity, and water contact angle measurements were all carried out. It was found out that graphene oxide was endowed with nontrivial photocatalytic activity by increasing its content in the nanocomposite (from 1/100 to 1/9, with respect to the dosage of nano TiO<sub>2</sub>). Overall, the nano TiO<sub>2</sub>-functionalized graphene oxide nanocomposite is a promising candidate in applications of environment remediation.

**Keywords** Nano TiO<sub>2</sub> · Graphene oxide · Photocatalyst · Environment remediation

## 1 Introduction

Nowadays, photodegradation of dyes in the effluents has drawn increasing attention for its wide applicability range, operational simplicity, high cost-

effectiveness, and green process (Hoffmann et al. 1995; Cheng et al. 2015; Rajeshwar et al. 2008). Among all photocatalysts, nano TiO<sub>2</sub>-based catalysts are most widely exploited. Nevertheless, more researches are needed in many aspects like enhancing the absorbability, light efficiency, and hydrophilicity (if in aqueous medium) (Asha et al. 2015; Inagaki et al. 2005; Kunacheva and Stuckey 2014; Woan et al. 2009). Graphene oxide (GO) has the same single-atomic sheet of sp<sup>2</sup> hybridized hexagonal skeleton as graphene. But, abundant oxygenic groups of GO (e.g., hydroxyl, carboxyl, carbonyl, epoxy, and alkoxy groups) give it better chemical reactivity and hydrophilicity, which allows GO to be easily modified to be versatile (Yuan et al. 2014; Zhang et al. 2014; Zhu et al. 2010). Hence, recombination of the NT with GO is anticipated to open up new possibilities for the photocatalysis technology.

Williams et al. (2008) realized the reduction of GO in ethanol by gaining electrons from ultraviolet (UV)-irradiated TiO<sub>2</sub> suspensions. This methodology offered a commerciological reduction technique of GO, but it still has a long way to go as the use of gold sputtered terminations. Qiu et al. (2014) reported a simple one-step hydrothermal method towards in situ growth of ultradispersed mesoporous TiO<sub>2</sub> nanocrystals with (001) facets on 3D-graphene aerogels. The TiO<sub>2</sub>/graphene aerogels exhibited a highly recyclable photocatalytic activity for methy orange pollutant and a high specific capacity in lithium-ion batteries. Heish et al. (2015) used the hydrothermal method to obtain Pt-TiO<sub>2</sub>/graphene photocatalysts, of which the photocatalytic

---

R. Wang · R. Yang · B. Wang (✉) · W. Gao  
State Key Laboratory of Pulp and Paper Engineering, South China  
University of Technology, Wushan Rd. Tianhe  
District Guangzhou 510640, China  
e-mail: febwang@scut.edu.cn

activity was excellent for degradation of acid orange 7 under visible light. Zhang et al. (2009) prepared a chemically bonded TiO<sub>2</sub> (P25)-graphene nanocomposite photocatalyst. Compared with the bare P25 and P25-CNTs, a significant enhancement in the reaction rate was observed with the as-prepared photocatalyst, though the photocatalysis performance could be further improved.

In this study, a potent photocatalyst was prepared by recombining NT with GO via a classic solvothermal process to achieve better absorbability, light efficiency, and hydrophilicity. The charge transfer and hydronium movement in the process were investigated to explore the possible mechanism, especially the active ions and frequent contacts between the catalyst and hydronium. In general, this photocatalyst is anticipated to broaden the utilizations of TiO<sub>2</sub>/carbon-based photocatalysts in sewerage treatments.

## 2 Experimental

All chemicals used in this study were used as received, without any further purification. All solutions were prepared using deionized water. The experiments were conducted at ambient temperature and humidity.

### 2.1 Synthesis of the Nanocomposite

First, graphene oxide (GO) was synthesized by the modified Hummers' method (Hummers and Offeman 1958). In brief, 6 g of graphite was put into a mixture of 120 mL of concentrated H<sub>2</sub>SO<sub>4</sub>, 5 g of K<sub>2</sub>S<sub>2</sub>O<sub>8</sub>, and 5 g of P<sub>2</sub>O<sub>5</sub> (Nethravathi and Rajamathi 2008). The solution was heated to 95 ± 3 °C and kept stirring for 5 h in an oil bath. Then the solution was cooled down and diluted to 500 mL with slowly adding deionized water. Followed by filtering using a cellulose ester membrane (pore size of 0.22 μm) and dehydrating under ambient condition, the pre-oxidized product was obtained. Thereafter, the product was further oxidized by Hummers and Offeman methods to produce the graphite oxide. After the exfoliation by simultaneously agitating and ultrasonically dispersing 0.1 mg/mL of graphite oxide dispersion for 1 h, the graphene oxide was recovered by filtration and air dry.

The nano TiO<sub>2</sub>-functionalized graphene oxide nanocomposite was obtained via a solvothermal method based on Rajamathi's work with modifications. In details, 40 mg of GO was dissolved in a solution of

deionized water (40 mL) and ethanol (20 mL) by ultrasonic treatment for 1 h. Then 0.36 g of NT was added in and stirring was continued for another 2 h to get a homogeneous suspension. Thereafter, the obtained suspension was placed in a stainless autoclave and held at 120 °C for 3 h to achieve the reduction of GO and the deposition of NT on the graphene sheet at the same time. Finally, the resulting nanocomposite was recovered by filtration and air drying.

### 2.2 Characterization

Powder X-ray diffraction (XRD) was performed on a Bruker D8-Advance X-ray diffractometer with monochromatized Cu Kα radiation (λ = 1.5418 Å). Raman spectra was investigated on a LabRAM Aramis Raman Spectrometer in the frequency range between 100 and 3500 cm<sup>-1</sup> with a resolution of 1 cm<sup>-1</sup>. Fourier transform infrared (FTIR) spectra were carried out using Bruker VERTEX 70 spectrometer in the frequency range of 3600–400 cm<sup>-1</sup> with a resolution of 4 cm<sup>-1</sup>. Specific surface areas (SSA) of all photocatalysts were measured at 77 K by Brunauer–Emmett–Teller (BET) nitrogen adsorption–desorption (Micromeritics ASAP 2020 Instrument). Field emission scanning electron microscope (FESEM) image was taken with a Zeiss LEO1530VP scanning electron microscope operated at 20 kV. The conductivity measurement was conducted with a DDSJ 308A conductivity meter every 10 min at ambient conditions for 50 min, and the solution concentration was fixed at 0.1 g/L. The UV-visible spectra of the photocatalysts were carried out using a UV-visible spectrophotometer (8453, Agilent) in the λ range from 200 to 900 nm. The water contact angle (WCA) of the photocatalysts were measured by a surface tension-contact angle tester (OCA40 Micro, Dataphysics) at ambient conditions; the three-phase interface is consist of air, photocatalyst solution, and glass slide.

### 2.3 Photocatalytic Experiments

The photodegradation of MB was measured according to the Lambert–Beer' law (Lambert 1760; Beer 1852). In a typical process, aqueous solutions of the MB (5 mg/L, 20 mL) and photocatalysts (NT/the blend/the nanocomposite, 2 mg) were placed in a 50-mL conical flask and a 10-min ultrasonic treatment was being proceeded. Under ambient conditions, the photoreaction vessel was exposed to the

**Fig. 1** **a** XRD patterns of GO, NT, and the nanocomposite in the range of 5–60°. **b** Raman spectra of NT, GO, and the nanocomposite in the range of 100–3500  $\text{cm}^{-1}$ . **c** Fourier transform infrared (FTIR) spectra of NT, GO, and the nanocomposite in the range of 3600–400  $\text{cm}^{-1}$

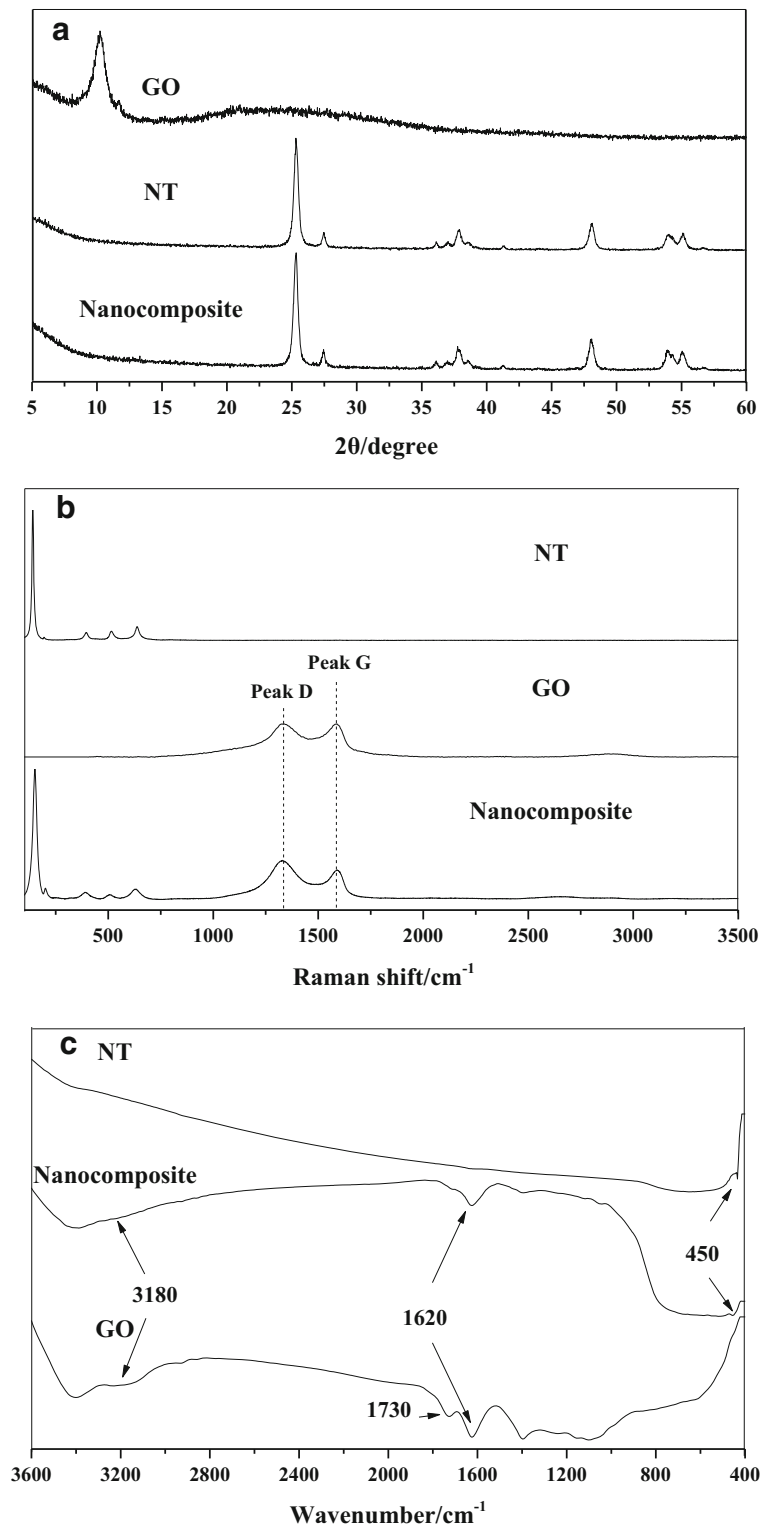
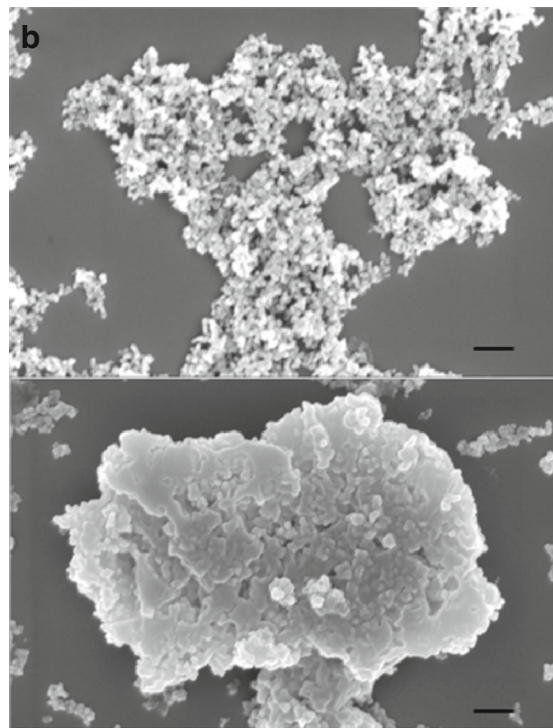
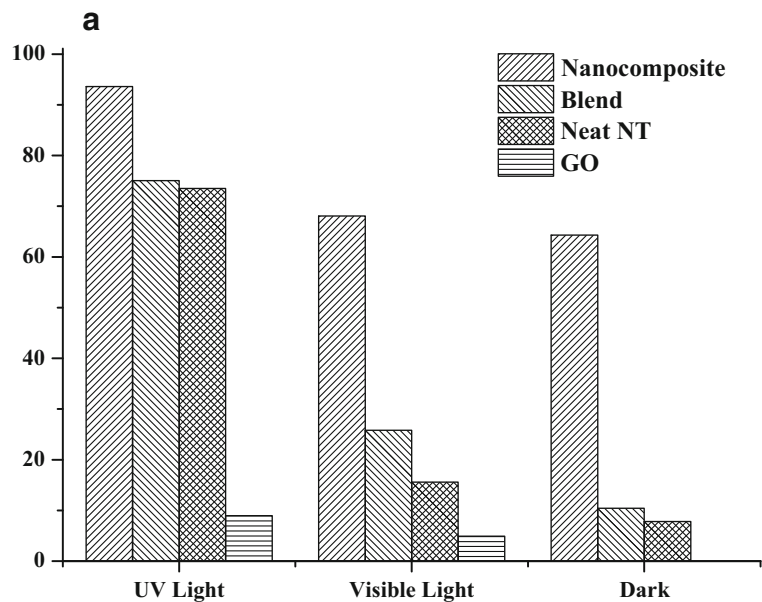


**Fig. 2 a** Photocatalysis experiments of methylene blue using neat NT, the NT/GO blend, and the nanocomposite under different illuminant (UV light, visible light, and in dark). **b** Field emission scanning electron microscope (FESEM) of NT (*above*) and the nanocomposite (*below*) based on mica plate. Scale bar, 200 nm



UV and visible-light irradiation, which were generated by an 8 W UV lamp (354 nm) and an 8 W white-light lamp (620 nm) with the same intensity of  $2 \text{ mW/cm}^2$ , respectively. The photocatalytic reaction was started by turning on the Hg lamp, and the whole system was shielded for 40 min. Then the

photoreacted solution was centrifuged, and the supernatant was analyzed by measuring the absorbance ( $\lambda_{\text{max}}=664 \text{ nm}$ ) on a UV-visible spectrometer (DR 2800, HACH). Dark adsorption test was adopted to compare the adsorptivity of NT, the blend, and the nanocomposite. In this test, 2 mg of photocatalyst

was dispersed in 20 mL of MB solution (5 mg/L) with ultrasonication and kept in the dark for 40 min. Then the absorbance of the dispersion was measured as mentioned above. From the absorbance changes before and after the degradation, the amount of dyes removed by the photocatalyst could be estimated.

### 3 Results and Discussion

#### 3.1 Characterization of the Nanocomposite

Figure 1a shows the XRD of NT and the nanocomposite, in which the latter is in line with NT, and there are no observed diffraction peaks for carbon species. Moreover, the sharp peak that represents the presence of GO around  $11^\circ$  is absent. Figure 1b shows the Raman characterizations. It reveals that NT is composed of anatase-TiO<sub>2</sub>, and the notable features for GO-added samples are the peak *D* ( $\sim 1331\text{ cm}^{-1}$ ) and peak *G* ( $\sim 1580\text{ cm}^{-1}$ ). In addition, the *D/G* intensity ratio is increased from 0.998 of GO to 1.315 of the nanocomposite. Figure 1c shows the FTIR spectra of samples. For the nanocomposite sample, it is evident that peaks at 450 and  $1620\text{ cm}^{-1}$  associate with anatase-TiO<sub>2</sub> and the graphene skeleton, respectively. Specifically, the absent adsorptive peak represents C=O stretching of –COOH at  $1730\text{ cm}^{-1}$  and weaker adsorption around  $3180\text{ cm}^{-1}$ , which relates to the carboxylic hydroxyl group. Therefore, the reduction of GO and chemical bonding between NT and GO during the process are verified (Iwashina et al. 2015; Li et al. 2014).

#### 3.2 Photocatalysis Experiments

Results of the photocatalysis experiments are shown in Fig. 2. It is obvious that under the UV light irradiation, the nanocomposite exhibits the highest dye removal percentage (denoted as *R%* in the following) as 93 %,  $\sim 20\%$  more than those of other photocatalysts. Specifically, the nanocomposite exhibited a degradation capacity of  $\sim 46.5\text{ mg/g}$  towards MB, which was quadruple of that of the P25-graphene composite photocatalyst (Zhang et al. 2009). In addition, when photocatalyst is out of use, *R%* under the UV irradiation is 9 %. The possibility of reusing the photocatalyst was also examined, and the *R%* stayed over 80 % after four apply–recycle

circle. This decrease might be owing to the irreversible coverage caused by dye molecules. In general, the high *R%* of the nanocomposite should be attributed to the following properties.

##### 3.2.1 Enhanced Adsorptivity

As displayed in Fig. 2a,  $\sim 64\%$  of *R%* value is garnered by the nanocomposite when unirradiated, which permits an excellent photocatalyst with high adsorption capacity of dye molecules (Zhang et al. 2008; Morales et al. 2008). And the best explanation for this was found to be its microscopic advantages. The BET SSA measurements and the FESEM images are shown in Table 1 and Fig. 2b, respectively. The nanocomposite is endowed with 38 % larger SSA and nanosize compared with NT, which is in discoid shape with dimensions ranging between 40 and 50 nm in width and 1 and 2 nm in height. Given these facts, a mechanism could be proposed as that NT particle bound with GO tuned the nanocomposite a specific microstructure allowing more dye molecules to fix on (Hasan et al. 2015; Xiang et al. 2015). It was indicated that GO played an important role for the increment in BET SSA, with respect to that reported by Zhang et al. (2009), whose value was around  $51.034\text{ m}^2\text{g}^{-1}$ , but with much less GO incorporation. Besides, vast conjugated structures of the nanocomposite commonly seen in aromatic dyes also made contributions (Shimizu et al. 2015).

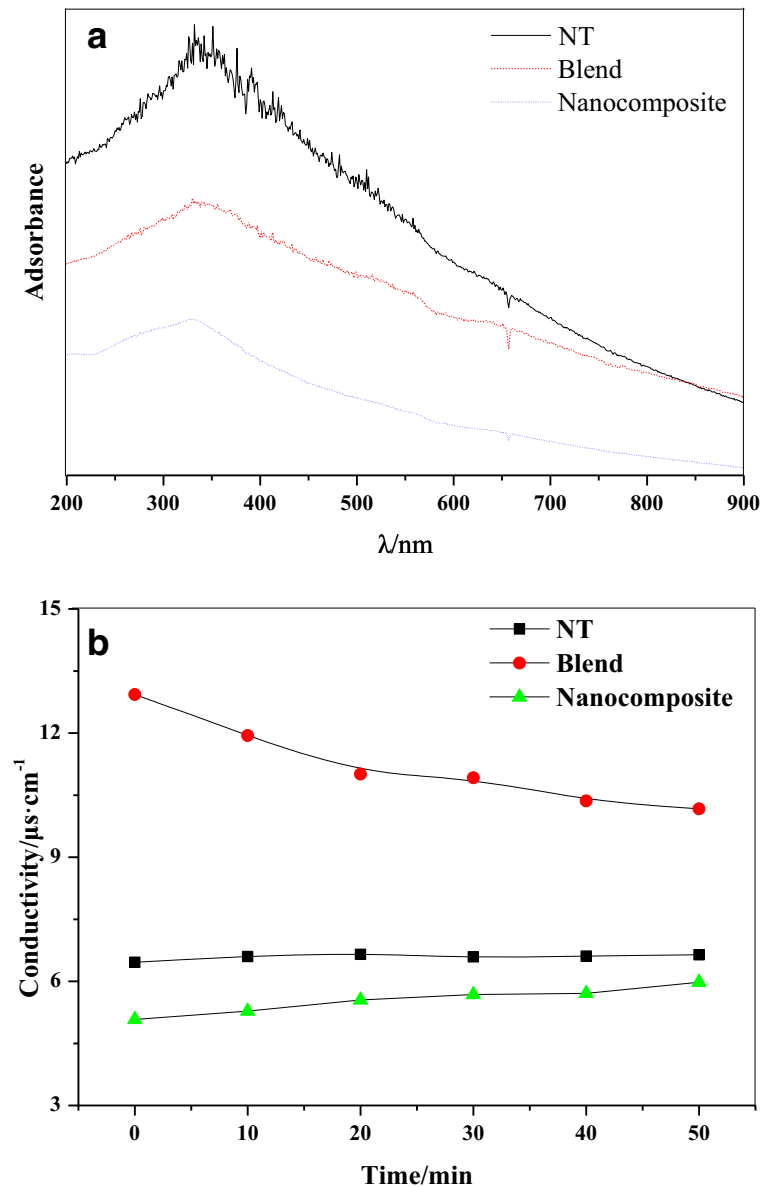
##### 3.2.2 High Light Efficiency

As it is shown in Fig. 3, the nanocomposite exhibits the lowest conductivity, and the most stable absorbance as the  $\lambda$  grows. And, in the photodegradation of visible light, 68 % of *R%* is exhibited by the nanocomposite, whereas the value for the mixture and pristine NT are only 25 and 15 %, respectively. Therefore, the ray was supposed to lose less energy

**Table 1** The BET surface area measurements of NT and the nanocomposite

	NT	Nanocomposite
Single point surface area at P/P <sub>0</sub> (m <sup>2</sup> /g)	41.2	56.08
BET surface area (m <sup>2</sup> /g)	40.46	55.66
Langmuir surface area (m <sup>2</sup> /g)	54.3	75.02

**Fig. 3** **a** The absorbance- $\lambda$  trend of neat NT, the NT/GO blend, and the nanocomposite in the  $\lambda$  range of 200–900 nm. **b** The conductivity-time measurements of neat NT, the NT/GO blend, and the nanocomposite in the concentration of 0.1 g/L

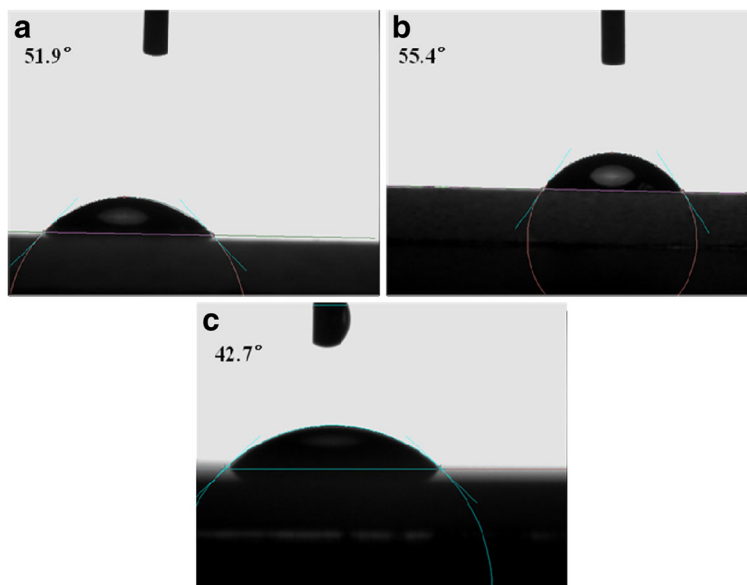


before arriving at the nanocomposite, and the highest light efficiency was confirmed (Tryba et al. 2004). However, this evidence was supported by the updated conjugate  $\pi$ -bond within the graphene skeleton by NT particles, which enlarged the extent of  $\pi$ -bond, thereafter decreasing the amount of free electrons related to the conductivity. Concurrently, more localized electrons in the nanocomposite would guarantee more photogeneration of electron-hole pair participation in the catalysis, even under visible-light irradiation (Ren et al. 2007; Sakthivel and Kisch 2003; Woan et al. 2009; Yang 1988).

### 3.2.3 Better Dispersity

The WCA measurement results of all samples are listed in Fig. 4. The nanocomposite expresses the smallest WCA, which equals to the most hydrophilic (Young 1805). It was found that the enhanced hydrophilicity was related to the more active O (in the updated Ti–O–C bonding) that had been stimulated by the positively charged Ti (Bharathidasan et al. 2015). On the other hand, the WCA increase was limited because the dominant graphene sheet was nonpolar. Although there was a compromise,

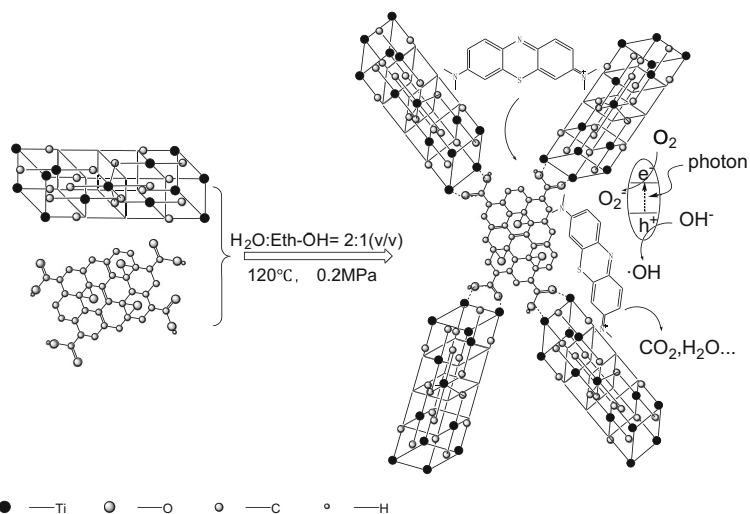
**Fig. 4** The contact angle measurements of neat NT (a), the NT/GO blend (b), and the nanocomposite (c) based on the three phases, which consist air, photocatalyst solution, and slide



the photoreaction efficiency was still promoted, as the incremental probability for dye molecules to react with radicals/ions (e.g., OH, O<sub>2</sub><sup>-</sup>) was generated by photocatalyst particles in water (as illustrated in Scheme 1).

#### 4 Conclusions

In summary, NT-functionalized GO nanocomposite with excellent photocatalysis performance has been readily prepared via a facile solvothermal process. The



**Scheme 1** Schematic structure of the nano TiO<sub>2</sub>-functionalized graphene oxide nanocomposite and its presumed processes of photodegrading the methylene blue. The TiO<sub>2</sub> nanoparticles are deposited on the graphene sheet, which plays important roles during the photocatalysis process, such as increases the photocatalyst's adsorptivity, weakens the photogenerated electron-hole pair to recombine, and improves its solubility in water. The methylene blue molecules was able to transfer from the solution to the catalysts' surface and be adsorbed via  $\pi$ - $\pi$  conjugation between the molecule and the aromatic regions on graphene

sheet, and increased BET surface area would therefore enhanced the adsorptivity for the nanocomposite when compared with bare nano TiO<sub>2</sub>; The reconstructed Ti-O-C bond of the nanocomposite render poorer conductivity and correspondingly lower loss of light energy, which facilitates the promotion in light utilization efficiency for the nanocomposite; simultaneously, the nonpolar  $\pi$ - $\pi$ -conjugated structure was modified, and the dispersity of the nanocomposite was improved in contrast to pristine nano TiO<sub>2</sub>, and broadens its practical applications

nanocomposite exhibited enhanced adsorptivity, light efficiency, and hydrophilicity. The nanocomposite had proven a better photocatalyst over bare NT in decomposing the MB under different illuminant irradiations (UV or visible light). Moreover, the  $R\%$  of the nanocomposite was higher than that of the NT/GO mixture, and the reconstructed Ti–O–C bond that altered the morphology maybe accountable for this issue. This study is anticipated to validate a different pathway to produce the NT/carbon-based nanocomposite as a photocatalyst, providing reference for present techniques in environment remediation.

**Acknowledgments** The authors would like to acknowledge the support of the National Science and Technology Support Plan (2013BAC01B03), the National Natural Science Foundation of China (B5141070) and the Natural Science Foundation of Guangdong Province (2015A030310369).

## References

- Asha, R., Vishnuganth, M. A., Remya, N., Selvaraju, N., & Kumar, M. (2015). Livestock wastewater treatment in batch and continuous photocatalytic systems: performance and economic analyses. *Water, Air, and Soil Pollution*, 226(5), 1–13.
- Beer, A. (1852). Bestimmung der absorption des rothen lichts in farbigen flüssigkeiten. *Annalen der Physik und Chemie*, 86(2).
- Bharathidasan, T., Narayanan, T. N., Sathyanaryanan, S., & Sreejakumari, S. (2015). Above 170° water contact angle and oleophobicity of fluorinated graphene oxide based transparent polymeric films. *Carbon*, 84, 207–213.
- Cheng, C., Kong, Z., & Khan, M. (2015). Photocatalytic-fenton degradation of glycerol solution over visible light-responsive  $\text{CuFe}_2\text{O}_4$ . *Water, Air, and Soil Pollution*, 226(10), 1–12.
- Hasan, M., Banerjee, A. N., & Lee, M. (2015). Enhanced thermo-optical performance and high BET surface area of graphene@ PVC nanocomposite fibers prepared by simple facile deposition technique:  $\text{N}_2$  adsorption study. *Journal of Industrial and Engineering Chemistry*, 21, 828–834.
- Hoffmann, M. R., Martin, S. T., Choi, W., & Bahnemann, D. W. (1995). Environmental applications of semiconductor photocatalysis. *Chemical Reviews*, 95(1), 69–96.
- Hsieh, H., Chen, J., & Wu, T. (2015). Pt-TiO<sub>2</sub>/graphene photocatalysts for degradation of AO7 dye under visible light. *Applied Surface Science*, 340, 9–17.
- Hummers, S., & Offeman, E. (1958). Preparation of graphitic oxide. *Journal of the American Chemical Society*, 80(6), 1339–1339.
- Inagaki, M., Kojin, F., Tryba, B., & Toyoda, M. (2005). Carbon-coated anatase: the role of the carbon layer for photocatalytic performance. *Carbon*, 43(8), 1652–1659.
- Iwashina, K., Iwase, A., Ng, Y. H., Amal, R., & Kudo, A. (2015). Z-schematic water splitting into H<sub>2</sub> and O<sub>2</sub> using metal sulfide as a hydrogen-evolving photocatalyst and reduced graphene oxide as a solid-state electron mediator. *Journal of the American Chemical Society*, 137(2), 604–607.
- Kunacheva, C., & Stuckey, D. C. (2014). Analytical methods for soluble microbial products (SMP) and extracellular polymers (ECP) in wastewater treatment systems: a review. *Water Research*, 61, 1–18.
- Lambert, J. (1760). *Photometria, sive de Mensura et gradibus luminis, colorum et umbrae*. Augsburg: Eberhard Klett.
- Li, S., Zhao, C., Shu, K., Wang, C., Guo, Z., Wallace, G., et al. (2014). Mechanically strong high performance layered polypyrrole nano fibre/graphene film for flexible solid state supercapacitor. *Carbon*, 79, 554–562.
- Morales, W., Cason, M., Aina, O., de Tacconi, N. R., & Rajeshwar, K. (2008). Combustion synthesis and characterization of nanocrystalline WO<sub>3</sub>. *Journal of the American Chemical Society*, 130(20), 6318–6319.
- Nethravathi, C., & Rajamathi, M. (2008). Chemically modified graphene sheets produced by the solvothermal reduction of colloidal dispersions of graphite oxide. *Carbon*, 46(14), 1994–1998.
- Qiu, B., Xing, M., & Zhang, J. (2014). Mesoporous TiO<sub>2</sub> nanocrystals grown in situ on graphene aerogels for high photocatalysis and lithium-ion batteries. *Journal of the American Chemical Society*, 136(16), 5852–5855.
- Rajeshwar, K., Osugi, M. E., Chanmanee, W., Chenthamarakshan, C. R., Zanon, M. V. B., Kajitvichyanukul, P., & Krishnan-Ayer, R. (2008). Heterogeneous photocatalytic treatment of organic dyes in air and aqueous media. *Journal of Photochemistry and Photobiology, C: Photochemistry Reviews*, 9(4), 171–192.
- Ren, W., Ai, Z., Jia, F., Zhang, L., Fan, X., & Zou, Z. (2007). Low temperature preparation and visible light photocatalytic activity of mesoporous carbon-doped crystalline TiO<sub>2</sub>. *Applied Catalysis B: Environmental*, 69(3–4), 138–144.
- Sakthivel, S., & Kisch, H. (2003). Daylight photocatalysis by carbon-modified titanium dioxide. *Angewandte Chemie International Edition*, 42(40), 4908–4911.
- Shimizu, H., Cojal González, J. D., Hasegawa, M., Nishinaga, T., Haque, T., Takase, M., et al. (2015). Synthesis, structures, and photophysical properties of  $\pi$ -expanded oligothiophene 8-mers and their satum-like C<sub>60</sub> complexes. *Journal of the American Chemical Society*, 137(11), 3877–3885.
- Tryba, B., Tsumura, T., Janus, M., Morawski, A. W., & Inagaki, M. (2004). Carbon-coated anatase: adsorption and decomposition of phenol in water. *Applied Catalysis B: Environmental*, 50(3), 177–183.
- Williams, G., Seger, B., & Kamat, P. V. (2008). TiO<sub>2</sub>-graphene nanocomposites. UV-assisted photocatalytic reduction of graphene oxide. *ACS Nano*, 2(7), 1487–1491.
- Woan, K., Pyrgiotakis, G., & Sigmund, W. (2009). Photocatalytic carbon-nanotube-TiO<sub>2</sub> composites. *Advanced Materials*, 21(21), 2233–2239.
- Xiang, Q., Lang, D., Shen, T., & Liu, F. (2015). Graphene-modified nanosized Ag<sub>3</sub>PO<sub>4</sub> photocatalysts for enhanced visible-light photocatalytic activity and stability. *Applied Catalysis B: Environmental*, 162, 196–203.
- Yang, E.S. (1988). *Microelectronics devices*. Mac Graw-Hill.
- Young, T. (1805). *An essay on the cohesion of fluids*. *Philosophical Transactions of the Royal Society of London* (pp. 65–87).



- Yuan, Y., Li, H., Luo, M., Qin, S., Luo, W., Li, L., et al. (2014). TiO<sub>2</sub>-mediated photodegradation of aqueous trinitrophenol irradiated by an artificial light source. *Water, Air, and Soil Pollution*, 225(3), 1–9.
- Zhang, W., Fu, B., & Zhu, F. (2008). Efficient TiO<sub>2</sub> photocatalysts from surface hybridization of TiO<sub>2</sub> particles with graphite-like carbon. *Advanced Functional Materials*, 18(15), 2180–2189.
- Zhang, H., Lv, X., Li, Y., Wang, Y., & Li, J. (2009). P25-graphene composite as a high performance photocatalyst. *ACS Nano*, 4(1), 380–386.
- Zhang, L., Liu, J., Dai, M., Zhou, F., & Liu, G. (2014). Adsorption of clofibric acid from aqueous solution by graphene oxide and the effect of environmental factors. *Water, Air, and Soil Pollution*, 225(8), 1–10.
- Zhu, Y., Murali, S., Cai, W., Li, X., Suk, J. W., Potts, J. R., et al. (2010). Graphene and graphene oxide: synthesis, properties, and applications. *Advanced Materials*, 22(35), 3906–3924.